01 Jan 2014

Strong-Randomness Infinite-Coupling Phase in a Random Quantum Spin Chain

Fawaz Hrahsheh

José A. Hoyos

Rajesh Narayanan

Thomas Vojta
Missouri University of Science and Technology, vojtat@mst.edu

Recommended Citation

F. Hrahsheh et al., "Strong-Randomness Infinite-Coupling Phase in a Random Quantum Spin Chain," *Physical review B: Condensed matter and materials physics*, vol. 89, no. 1, American Physical Society (APS), Jan 2014.
The definitive version is available at https://doi.org/10.1103/PhysRevB.89.014401

Strong-randomness infinite-coupling phase in a random quantum spin chain

Fawaz Hrahsheh,[1] José A. Hoyos,[2] Rajesh Narayanan,[3] and Thomas Vojta[1]
[1]*Department of Physics, Missouri University of Science and Technology, Rolla, Missouri 65409, USA*
[2]*Instituto de Física de São Carlos, Universidade de São Paulo, Caixa Postale 369, CEP 13560-970 São Carlos, São Paulo, Brazil*
[3]*Department of Physics, Indian Institute of Technology Madras, Chennai 600036, India*
(Received 28 October 2013; published 3 January 2014)

We study the ground-state phase diagram of the Ashkin-Teller random quantum spin chain by means of a generalization of the strong-disorder renormalization group. In addition to the conventional paramagnetic and ferromagnetic (Baxter) phases, we find a partially ordered phase characterized by strong randomness and infinite coupling between the colors. This unusual phase acts, at the same time, as a Griffiths phase for two distinct quantum phase transitions, both of which are of infinite-randomness type. We also investigate the quantum multicritical point that separates the two-phase and three-phase regions, and we discuss generalizations of our results to higher dimensions and other systems.

DOI: 10.1103/PhysRevB.89.014401 PACS number(s): 75.10.Nr, 75.40.−s, 05.70.Jk

I. INTRODUCTION

Random quantum many-particle systems are easiest to understand if both interactions and disorder are weak. In these cases, the system often behaves analogously to a clean noninteracting one, with small perturbative corrections. If, on the other hand, interactions or disorder are strong, qualitatively new behavior can arise. For instance, repulsive interactions induce a new phase, the Mott insulator, in systems of lattice bosons or electrons. Moreover, strong randomness leads to an Anderson insulator in which the quantum wave functions are localized.

Particularly strong disorder and correlation effects can be expected in the vicinity of zero-temperature quantum phase transitions where the fluctuations extend over large length and time scales. Examples include infinite-randomness criticality [1,2], quantum Griffiths singularities [3,4], and smeared phase transitions [5] (for recent reviews see, e.g., Refs. [6,7]).

Disordered quantum spin chains are a paradigmatic class of materials to study these phenomena, both in theory and in experiment. Theoretically, they have been attacked by strong-disorder renormalization group (SDRG) methods [8,9] that give asymptotically exact results for a number of one-dimensional systems. The ground state of the antiferromagnetic spin-1/2 random quantum Heisenberg chain is an exotic random-singlet state controlled by an infinite-randomness renormalization group fixed point [10]. Similarly, the ferromagnetic-paramagnetic quantum phase transition of the random transverse-field Ising chain is of unconventional infinite-randomness type and accompanied by power-law quantum Griffiths singularities [2]. Some of these phenomena have been observed in early experiments on organic crystals [11,12] and more recently in $MgTiOBO_3$ [13].

In this paper we investigate the random quantum Ashkin-Teller model, a prototypical disordered spin chain (or ladder) that can be understood as two coupled random quantum Ising chains. In addition to quantum spin systems, versions of the Ashkin-Teller model are used to describe layers of atoms absorbed on surfaces [14], current loops in high-T_c superconductors [15], as well as the elastic response of DNA molecules [16].

We explore the ground-state phase diagram of the random quantum Ashkin-Teller chain by a generalization of the SDRG technique. In addition to the conventional paramagnetic and ferromagnetic phases, we identify an unconventional partially ordered phase characterized by finite but strong randomness and infinite coupling between the two constituent Ising chains (see Fig. 1). It plays the role of a "double Griffiths" phase for two separate quantum phase transitions both of which are of infinite-randomness type. The two-phase region at weak coupling and the three-phase region at strong coupling are separated by a distinct infinite-randomness multicritical point.

The remainder of this paper is organized as follows. We introduce the random quantum Ashkin-Teller model in Sec. II. The SDRG method is developed in Sec. III. Section IV is devoted to the resulting ground-state phase diagram and the properties of the quantum phase transitions between the different phases. In the concluding Sec. V, we discuss generalizations of our results to higher dimensions as well as connections to other random quantum systems.

II. RANDOM QUANTUM ASHKIN-TELLER MODEL

The Hamiltonian of the one-dimensional random quantum Ashkin-Teller model is given by [17–19]

$$H = -\sum_{\alpha=1}^{2}\sum_{i}\left(J_i S^z_{\alpha,i} S^z_{\alpha,i+1} + h_i S^x_{\alpha,i}\right) - \sum_{i}\left(K_i S^z_{1,i} S^z_{1,i+1} S^z_{2,i} S^z_{2,i+1} + g_i S^x_{1,i} S^x_{2,i}\right), \quad (1)$$

where S^x and S^z denote the usual Pauli matrices. The model can be understood as two identical random transverse-field Ising chains [first line of Eq. (1)], coupled via their energy densities [second line of Eq. (1)]. The index $\alpha = 1,2$ that distinguishes the two chains is often called the color index. The strength of the coupling between the colors can be parametrized by the ratios $\epsilon_{h,i} = g_i/h_i$ and $\epsilon_{J,i} = K_i/J_i$. Note that the Hamiltonian (1) is invariant under the duality transformation: $S^z_{\alpha,i} S^z_{\alpha,i+1} \to \tau^x_{\alpha,i}$, $S^x_{\alpha,i} \to \tau^z_{\alpha,i}\tau^z_{\alpha,i+1}$, $J_i \rightleftarrows h_i$, and $\epsilon_{J,i} \rightleftarrows \epsilon_{h,i}$, where τ^x and τ^z are the dual Pauli operators.

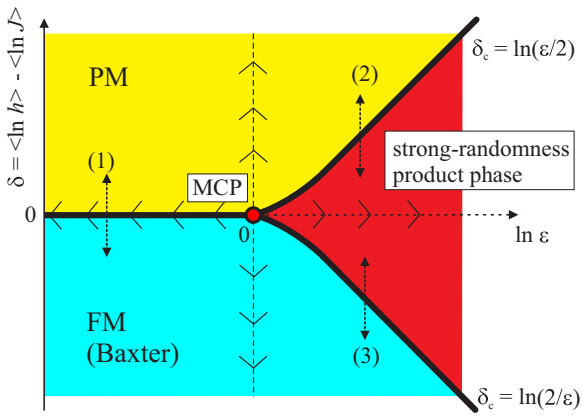

FIG. 1. (Color online) Schematic ground-state phase diagram of the random quantum Ashkin-Teller chain. For $\epsilon < 1$, the paramagnetic and ferromagnetic phases are connected by a direct continuous quantum phase transition. For $\epsilon > 1$, they are separated by a partially ordered "product" phase characterized by strong randomness and renormalization group flow towards infinite coupling. The flow is indicated by arrows on the principal axis, $\delta = 0$ and $\epsilon = 1$, of the multicritical point (MCP).

We take the interactions J_i and transverse fields h_i to be independent random variables. Without loss of generality, we can assume the J_i and h_i to be positive as possible negative signs can be absorbed by local transformations of the spin variables. For now, we assume the (bare) coupling strengths to be uniform, $\epsilon_{h,i} = \epsilon_{J,i} = \epsilon_I \geqslant 0$ [20]. Effects of random ϵ are discussed later in Sec. IV C.

The behavior of the random quantum Ashkin-Teller chain (1) in the weak-coupling regime, $\epsilon < \epsilon_c = 1$, has been studied in Refs. [19,21]. In the following, we therefore focus on the strong-coupling case, $\epsilon \geqslant \epsilon_c = 1$, where these results do not apply. For strong coupling, the terms in the second line of Eq. (1) dominate. It is thus convenient to introduce the product $S^z_{1,i} S^z_{2,i}$ as a new variable. We define

$$\sigma^z_i = S^z_{1,i} S^z_{2,i}, \tag{2}$$

$$\eta^z_i = S^z_{1,i}, \tag{3}$$

$$\sigma^z_i \eta^z_i = S^z_{2,i}. \tag{4}$$

The mapping of the Pauli matrices $S^x_{1,i}$ and $S^x_{2,i}$ can be easily worked out by exploring their action on a complete set of basis states in the four-dimensional single-site Hilbert space. This gives

$$\sigma^x_i = S^x_{2,i}, \tag{5}$$

$$\eta^x_i = S^x_{1,i} S^x_{2,i}, \tag{6}$$

$$\sigma^x_i \eta^x_i = S^x_{1,i}. \tag{7}$$

Using these transformations, the Hamiltonian (1) can be rewritten as

$$H = -\sum_i \left(K_i \sigma^z_i \sigma^z_{i+1} + h_i \sigma^x_i\right) - \sum_i \left(J_i \eta^z_i \eta^z_{i+1} + g_i \eta^x_i\right) - \sum_i \left(J_i \sigma^z_i \sigma^z_{i+1} \eta^z_i \eta^z_{i+1} + h_i \sigma^x_i \eta^x_i\right). \tag{8}$$

This form immediately gives an intuitive physical picture of the strong-coupling regime $\epsilon \gg 1$ close to self-duality, $h_{\rm typ} \approx J_{\rm typ}$, i.e., close to the horizonal line $\delta = 0$ in Fig. 1. Here, the typical values of the fields and interactions are defined as $\ln h_{\rm typ} = \langle \ln h \rangle$ and $\ln J_{\rm typ} = \langle \ln J \rangle$ where $\langle \cdots \rangle$ denotes the disorder average. The behavior of the product variable σ is dominated by the four-spin interactions K_i while the behavior of the variable η_i which traces the original spins is dominated by the two-spin transverse fields g_i. Moreover, the coupling terms between σ and η are weak. Thus, we expect the system to be in a phase in which the product variables σ_i develop long-range order while the spins remain disordered.

III. STRONG-DISORDER RENORMALIZATION GROUP

To confirm this intuitive picture and to work out the properties of the product phase and its transitions, we now develop a strong-coupling SDRG. The basic idea of any SDRG consists in identifying the largest local energy scale and perturbatively integrating out the corresponding high-energy degree of freedom. As the random quantum Ashkin-Teller model contains four competing local energies J_i, K_i, h_i, g_i rather than the usual two, we need to generalize the renormalization group (RG) scheme by also considering the second-largest energy in a local cluster. Details of this calculation are outlined in Appendix A. In the strong-coupling regime, $\epsilon > 1$, there are four possible SDRG steps:

(a) If the largest energy in the system is the two-spin field g_i, and the second largest energy in the local cluster of sites $i-1, i$ and $i+1$ is a four-spin interaction, say K_i, the SDRG step decimates the variable η_i but merges σ_i and σ_{i+1} to a new cluster $\tilde{\sigma}$. The unperturbed Hamiltonian for this SDRG step reads $H_0 = -K_i \sigma^z_i \sigma^z_{i+1} - g_i \eta^x_i$. We now keep only the ground state of H_0 and treat all other terms that contain σ_i, σ_{i+1} or η_i in second-order perturbation theory. The resulting Hamiltonian has the same form as Eq. (8) with one fewer site and renormalized energies arranged as shown in Fig. 2:

$$\tilde{J}_{\rm eff} = \frac{2 J_{i-1} J_i}{g_i}, \quad \tilde{h}_{\rm eff} = \frac{2 h_i h_{i+1}}{K_i} \tag{9}$$

As $\tilde{J}_{\rm eff}$ and $\tilde{h}_{\rm eff}$ are renormalized downward while all remaining K_i and g_i are unchanged, the coupling strengths $\epsilon_{h,i}$ and $\epsilon_{J,i}$ increase under renormalization.

(b) The same SDRG step is carried out if the largest energy is the four-spin interaction K_i and the second-largest energy in the cluster of sites i and $i+1$ is a two-spin field, say g_i.

(c) If the largest energy in the system is the two-spin field g_i, and the second largest energy in the local cluster of sites $i-1, i$ and $i+1$ is the field h_i, both σ_i and η_i are decimated. This is equivalent to decimating both original spins $S_{1,i}$ and

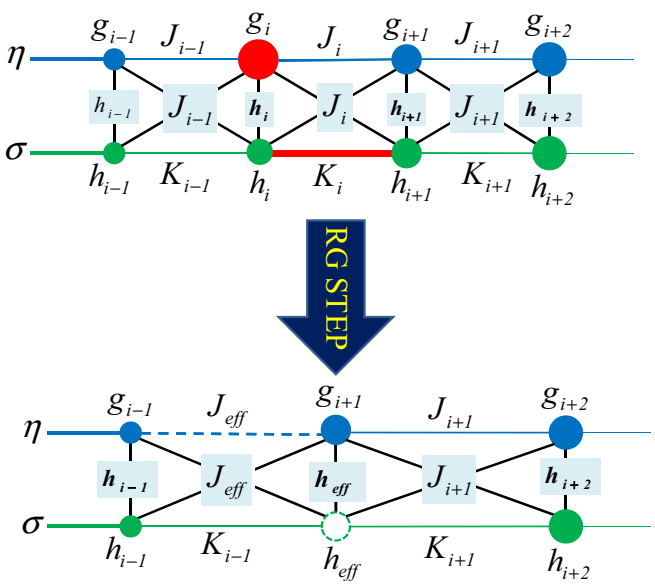

FIG. 2. (Color online) SDRG steps (a) and (b) decimate a spin variable η_i but merge two product variables, σ_i and σ_{i+1}, into a new cluster.

$S_{2,i}$ and leads to the recursion relations

$$\tilde{K}_{\rm eff} = \frac{K_{i-1}K_i}{2h_i}, \quad \tilde{J}_{\rm eff} = \frac{J_{i-1}J_i}{g_i + h_i} \tag{10}$$

for the interaction energies that emerge between sites $i-1$ and $i+1$ in the renormalized chain. This implies that the renormalized coupling strength $\tilde{\epsilon}_J = \epsilon_{J,i-1}\epsilon_{J,i}(1+\epsilon_{h,i})/2$ increases under renormalization (as we are interested in the strong-coupling regime $\epsilon > \epsilon_c = 1$).

(d) Finally, if the largest energy is the four-spin interaction K_i, and the second-largest energy associated with the sites i and $i+1$ is the interaction J_i, clusters are formed from σ_i and σ_{i+1} as well as η_i and η_{i+1}. This is equivalent to forming clusters of both original spin variables, $S_{1,i}$ and $S_{1,i+1}$ as well as $S_{2,i}$ and $S_{2,i+1}$. The resulting recursions for the transverse field $\tilde{h}_{\rm eff}$ and two-spin field $\tilde{g}_{\rm eff}$ acting on these clusters read

$$\tilde{g}_{\rm eff} = \frac{g_i g_{i+1}}{2J_i}, \quad \tilde{h}_{\rm eff} = \frac{h_i h_{i+1}}{K_i + J_i}. \tag{11}$$

The renormalized coupling strength $\tilde{\epsilon}_h = \epsilon_{h,i}\epsilon_{h,i+1}(1+\epsilon_{J,i})/2$ increases under renormalization.

The SDRG steps (a)–(d) are now iterated. As a result, the maximum local energy Ω in the system gradually decreases from its initial (bare) value Ω_I.

IV. PHASE DIAGRAM AND PHASE TRANSITIONS

A. Double Griffiths phase

Based on the SDRG recursions (9)–(11), the phase diagram of the random quantum Ashkin-Teller model shown in Fig. 1 is easily understood. Let us start by recalling that in the weak-coupling regime, $\epsilon < 1$, the local coupling strengths $\epsilon_{h,i}$ and $\epsilon_{J,i}$ decrease without limit under renormalization [19,21]. This implies that the two Ising chains that make up the Ashkin-Teller model decouple in the low-energy limit. Our system thus behaves analogously to the random transverse-field Ising chain [1,2]: A paramagnetic phase at large transverse fields h_i and a ferromagnetic phase at large interactions J_i are directly connected by an infinite-randomness critical point at $\delta = \ln h_{\rm typ} - \ln J_{\rm typ} = 0$ (transition 1 in Fig. 1) [22].

To understand the strong-coupling regime $\epsilon > 1$, let us first focus on the self-duality line $\delta = \ln h_{\rm typ} - \ln J_{\rm typ} = 0$. If the bare ϵ_I is just slightly above 1, most of the recursions will initially be site and bond decimations [types (c) and (d)]. In these steps, the local coupling strengths $\epsilon_{h,i}$ and $\epsilon_{J,i}$ rapidly increase. When they become larger than the widths of the J and h distributions, the character of the SDRG changes. Now, most steps are "mixed steps" of types (a) and (b). As a result, the product variable σ forms larger and larger clusters while the spin variable η is decimated.

The system is thus in a "double Griffiths phase": The σ part of the Hamiltonian behaves analogously to an ordered Griffiths phase while the η part behaves as in a disordered Griffiths phase. This double Griffiths phase has a nonzero product order parameter or polarization $M_p = \sum_i \sigma_i^z$ while the spin variable η_i^z (and thus $S_{1,i}^z$ and $S_{2,i}^z$) remains disordered, $M = \sum_i \eta_i^z = 0$. Note that this behavior is valid not just on the self-duality line, $\delta = 0$, but also in its vicinity because the RG flow of each of the variables σ and η is dominated by a single term in the Hamiltonian and does not rely on the balance between interactions and transverse fields. Thus, we have indeed discovered a bulk phase rather than a special line in the phase diagram. Moreover, as the $\epsilon_{h,i}$ and $\epsilon_{J,i}$ flow to infinity, the analysis is asymptotically exact.

To find the extensions of the partially ordered double Griffiths phase we need to locate its transitions to the conventional paramagnetic and ferromagnetic phases. Looking at the first sum in the Hamiltonian (8), it is clear that the long-range order of the product variable will be destroyed if we raise $\delta = \ln h_{\rm typ} - \ln J_{\rm typ}$ until the transverse fields h_i compete with the four-spin interactions K_i. This leads to a competition between the SDRG steps (a) and (c). From comparing the h recursion in Eqs. (9) with the K recursion in Eqs. (10), we conclude that the phase boundary between the double Griffiths phase and the paramagnetic phase (transition 2 in Fig. 1) is located at $K_{\rm typ} = 2h_{\rm typ}$ or equivalently $\delta_c = \ln(\epsilon/2)$ in the limit of large ϵ. Moreover, the transition is governed by an infinite-randomness fixed point in the random transverse-field Ising universality class. The phase boundary to the ferromagnetic phase (transition 3 in Fig. 1) can be found analogously. For large ϵ, it is located at $2J_{\rm typ} = g_{\rm typ}$ or equivalently $\delta_c = \ln(2/\epsilon)$ in agreement with the self-duality of the Hamiltonian.

The thermodynamics of the double Griffiths phase is highly unusual. It can be found in the usual way, i.e., by including conjugate fields in the SDRG. Each of the two order parameters, the magnetization $M = \sum_i \eta_i$ and the polarization $M_p = \sum_i \sigma_i^z$, displays power-law quantum Griffiths singularities controlled by different Griffiths dynamical exponents z_m and z_p, respectively, that vary nonuniversally with ϵ and δ. The exponent z_m diverges at the transition to the ferromagnetic phase while z_p diverges at the transition to the paramagnetic phase. Duality imposes the relation $z_p(\epsilon,\delta) = z_m(\epsilon,-\delta)$. Thermal quantities such as the entropy and the specific heat pick up contributions from both order parameters. Their Griffiths dynamical exponent $z = \max(z_m, z_p)$ thus displays

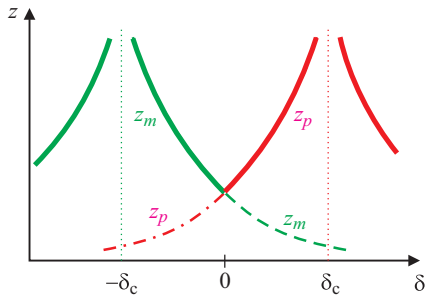

FIG. 3. (Color online) Schematic of the Griffiths dynamical exponent z as a function of δ for fixed $\epsilon > 1$. Rare large magnetization clusters lead to Griffiths singularities associated with the exponent z_m (green dashed line) while the singularities stemming from rare polarization clusters are associated with z_p (red dash-dotted line). Thermal quantities are dominated by the larger of the two exponents $z = \max(z_m, z_p)$ which features nonmonotonous behavior (thick solid line).

an interesting nonmonotonous dependence on δ, as sketched in Fig. 3.

B. Multicritical point

Finally, we consider the infinite-randomness multicritical point (MCP) located at $\epsilon = 1, \delta = 0$. It has two independent unstable directions, the lines $\delta = 0$ and $\epsilon = 1$. On the line $\epsilon = 1$ that separates the weak-coupling and strong-coupling regimes, all SDRG steps are site and bond decimations [types (c) or (d)]. The recursions (10) and (11) reduce to the well-known transverse-field Ising forms $\tilde{J}_{\text{eff}} = J_{i-1}J_i/(2h_i)$ and $h_{\text{eff}} = h_i h_{i+1}/(2J_i)$ [23]. The SDRG flow of the J and h distributions on the line $\epsilon = 1$ is thus identical to the corresponding flow of the random-transverse-field Ising chain. We emphasize, however, that although the SDRG flow of the J and h distributions at $\epsilon = 1$ is identical to the weak-coupling regime $\epsilon < 1$, the fixed-point Hamiltonian differs because the two Ising chains that make up the Ashkin-Teller model do not decouple.

The flow along the line $\epsilon = 1$ can be characterized by the following critical singularities: correlation length $\xi \sim |\delta|^{-\nu}$, magnetization $M \sim |\delta|^{\beta}$, and correlation time $\ln \xi_t \sim \xi^{\psi}$ with exponents

$$\nu = 2, \quad \beta = 2 - (1+\sqrt{5})/2 = 0.382, \quad \psi = 1/2. \tag{12}$$

In contrast, the SDRG flow on the self-duality line $\delta = 0$ for $\epsilon > 1$ close to the MCP is determined by the evolution of ϵ under repeated site and bond decimations [steps (c) and (d)]. It can be worked out (see Appendix B) by including $\ln(\epsilon)$ as an auxiliary variable in the SDRG flow of the J and h distributions. We find different critical singularities $\xi \sim (\epsilon - 1)^{-\nu_\epsilon}$ and $M_p \sim (\epsilon - 1)^{\beta_\epsilon}$ with exponents

$$\nu_\epsilon = \frac{8}{1+\sqrt{7}} = 2.194, \quad \beta_\epsilon = \frac{6-2\sqrt{5}}{1+\sqrt{7}} = 0.419. \tag{13}$$

The tunneling exponent ψ remains 1/2. Combining these results to write a scaling form of the polarization gives

$$M_p(\delta, \epsilon - 1) = b^{-\beta/\nu} M_p(\delta b^{1/\nu}, (\epsilon - 1) b^{1/\nu_\epsilon}), \tag{14}$$

where b is an arbitrary scale factor. The phase transition between the partially ordered and paramagnetic phases corresponds to a singularity of M_p for $\delta > 0$ and $\epsilon > 1$. Using Eq. (14), we find that the phase boundary behaves as

$$\delta_c \sim (\epsilon - 1)^{\nu_\epsilon/\nu} = (\epsilon - 1)^{4/(1+\sqrt{7})} = (\epsilon - 1)^{1.097} \tag{15}$$

sufficiently close to the multicritical point. The phase boundary to the ferromagnetic phase can be found analogously.

C. Random coupling strength ϵ

So far, we have considered systems in which the (bare) coupling strengths are uniform $\epsilon_{J,i} = \epsilon_{h,i} = \epsilon_I$. In the present section, we discuss what changes for random coupling strengths.

If *all* $\epsilon_{J,i}$ and $\epsilon_{h,i}$ are below the multicritical value of 1, the renormalized values $\tilde{\epsilon}$ are also smaller than 1 and decrease under renormalization. Thus, the two Ising chains that make up the Ashkin-Teller model decouple in the low-energy limit, just as in the case of uniform bare ϵ. Conversely, if *all* $\epsilon_{J,i}$ and $\epsilon_{h,i}$ are above the multicritical value of 1, the renormalized values $\tilde{\epsilon}$ are also larger than 1 and increase under renormalization. The system thus flows to the strong-coupling region, also just as in the case of uniform bare ϵ. Consequently, none of our results changes in these two cases, except for unimportant modifications of nonuniversal quantities. This also implies that the three bulk phases shown in Fig. 1 are stable against weak randomness in ϵ. The same holds for the phase transitions (1), (2), and (3) sufficiently far away from the multicritical point discussed in Sec. IV B.

In contrast, the multicritical point at $\delta = 0, \epsilon = 1$ itself is unstable against weak disorder in the $\epsilon_{J,i}$ and $\epsilon_{h,i}$. To show this, we analyze how the width of a narrow ϵ distribution around $\epsilon = 1$ flows under repeated SDRG site and bond decimations. By including $\ln \epsilon$ as an auxiliary variable in the SDRG and using the methods of Ref. [10], we find

$$\sigma_{\ln \epsilon} \sim \Gamma^{\phi_{1/2}^{(\text{sym})}}, \quad \phi_{1/2}^{(\text{sym})} = \frac{1+\sqrt{6}}{4}. \tag{16}$$

(Note that we need to consider the flow of a *symmetrically* distributed auxiliary variable; the exponent is therefore denoted as $\phi^{(\text{sym})}$.) This means that a narrow bare distribution broadens under the SDRG, destabilizing the uniform-ϵ multicritical point of Sec. IV B.

We have not found an analytic solution of the multicritical behavior in the case of random $\epsilon_{J,i}$ and $\epsilon_{h,i}$. Instead, we implement the SDRG numerically. We study systems with up to 5×10^8 sites. To place the system on the self-duality line $\delta = \ln h_{\text{typ}} - \ln J_{\text{typ}} = 0$, we employ identical power-law distributions $P_I(J) = J^{-1+1/w}/w$ and $R_I(h) = h^{-1+1/w}/w$ for the interactions and transverse fields, with w being a measure of the disorder. The coupling strengths $\ln \epsilon$ are drawn from a box distribution between $\ln \epsilon_{\min}$ and $\ln \epsilon_{\max}$. The results of a strongly disordered ($w = 2000$) example system are summarized in Figs. 4 and 5. We fix $\ln \epsilon_{\min} = -1000$ and tune the multicritical point by varying $\ln \epsilon_{\max}$. The data are averages over 50 different chains of 5×10^7 sites each. Figure 4 shows how the average $\langle \ln \epsilon \rangle$ and standard deviation $\sigma_{\ln \epsilon}$ of the coupling strength evolve under the SDRG. From the inset, we determine the multicritical point to be located

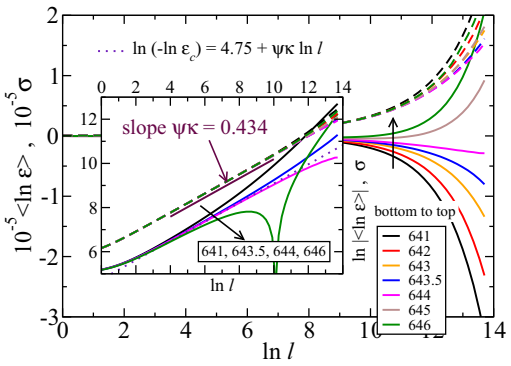

FIG. 4. (Color online) Average value $\langle \ln \epsilon \rangle$ (solid lines) and standard deviation $\sigma_{\ln \epsilon}$ (dashed lines) of the coupling strength $\ln \epsilon$ versus the SDRG length scale $\ln \ell$ for different values of the tuning parameter $\ln \epsilon_{\max} = 641, \ldots, 646$. The inset shows $\ln |\langle \ln \epsilon \rangle|$ and $\ln \sigma_{\ln \epsilon}$ for selected curves, giving a multicritical value of $\ln \epsilon_c = 643.75$.

between $\ln \epsilon_{\max} = 643.5$ and 644. Moreover, $\sigma_{\ln \epsilon}$ increases as $\ell^{\psi\kappa}$ with $\psi\kappa = 0.434(3)$ with the SDRG length scale. Here, the number in parentheses gives the error of the last digit. This error is mostly due to the uncertainty in precisely locating the multicritical point. The statistical error is much smaller. As the tunneling exponent remains at $\psi = 1/2$, this implies

$$\sigma_{\ln \epsilon} \sim \Gamma^{\kappa}, \quad \kappa = 0.868(6). \tag{17}$$

The value of the exponent κ (Ref. [24]) fulfills the constraint $\kappa < 1$ derived by Fisher [10]. Interestingly, it is not very different from the value $\phi_{1/2}^{(\mathrm{sym})} \approx 0.8624$ that describes the initial increase of $\sigma_{\ln \epsilon}$ near the uniform-ϵ multicritical point.

In Fig. 5, we study how the distance $|\langle \ln \epsilon \rangle - \ln \epsilon_c|$ from the multicritical point increases with SDRG length scale ℓ in the regime $|\langle \ln \epsilon \rangle - \ln \epsilon_c| < \sigma_{\ln \epsilon}$. We find $|\langle \ln \epsilon \rangle - \ln \epsilon_c| \sim \ell^{\psi(\kappa+\lambda)}$ with $\psi(\kappa + \lambda) = 0.89(2)$ [25]. Expressed in terms of Γ, this means

$$|\langle \ln \epsilon \rangle - \ln \epsilon_c| \sim \Gamma^{\kappa+\lambda}, \qquad \kappa + \lambda = 1.78(4). \tag{18}$$

Again, the error is mostly due to uncertainties in the location of the multicritical point as well as the fit range.

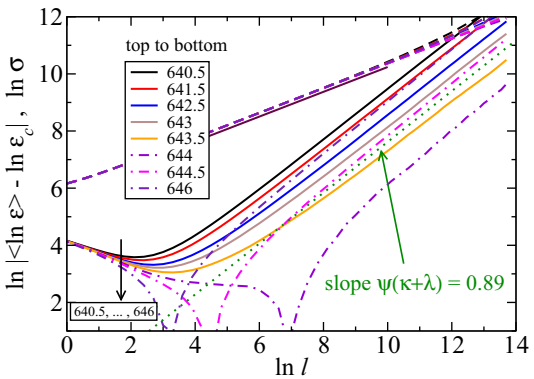

FIG. 5. (Color online) Distance $\ln |\langle \ln \epsilon \rangle - \ln \epsilon_c|$ from the multicritical point versus the SDRG length scale $\ln \ell$ for different values of the tuning parameter $\ln \epsilon_{\max} = 640.5, \ldots, 646$.

We have performed analogous calculations for a number of different parameter sets. For the weaker disorder case of $w = 3$ and $\ln \epsilon_{\min} = -3$, the multicritical point is located at $\ln \epsilon_{\max} \approx 2.424$. In this case, our analysis of 180 chains of 5×10^8 sites gives the same value as above, $\kappa\psi = 0.434(3)$. The exponent $\psi(\kappa + \lambda)$ is somewhat harder to determine in the weak-disorder case because the available fit range becomes very narrow. We find $\psi(\kappa + \lambda) = 0.88(4)$ in agreement with the strong-disorder value. Further calculations for even weaker disorder and shorter chains (between 1×10^6 and 5×10^7 sites) are less precise but compatible with the values given above.

Once $|\langle \ln \epsilon \rangle - \ln \epsilon_c| > \sigma_{\ln \epsilon}$, almost all ϵ are on the same side of the multicritical point. The further analysis therefore follows the steps outlined in Appendix B. The resulting multicritical behavior along the self-duality line on the strong-coupling side of the MCP is characterized by the power laws $\xi \sim (\langle \ln \epsilon \rangle - \ln \epsilon_c)^{-\nu_\epsilon}$ and $M_p \sim (\langle \ln \epsilon \rangle - \ln \epsilon_c)^{\beta_\epsilon}$ with exponents

$$\begin{aligned} \nu_\epsilon &= \frac{4 - 2\kappa}{\lambda} = 2.48(15), \\ \beta_\epsilon &= \frac{2 - \kappa}{\lambda}(2 - \phi_0) = 0.474(20). \end{aligned} \tag{19}$$

The shape of the phase boundary close to the multicritical point can be found as in Sec. IV B yielding $\delta_c \sim (\langle \ln \epsilon \rangle - \ln \epsilon_c)^{1.24}$.

V. DISCUSSION AND CONCLUSIONS

In summary, we have investigated the ground-state phase diagram of the random quantum Ashkin-Teller spin chain. The topology of the phase diagram, shown in Fig. 1, is analogous to that of the clean quantum Ashkin-Teller model (see, e.g., Ref. [26]). However, the properties of the phases and phase transitions are different. In addition to the usual paramagnetic and ferromagnetic phases, we have identified a partially ordered phase characterized by strong randomness and infinite coupling between the colors. This phase acts as a Griffiths phase for two distinct quantum phase transitions leading to an unconventional nonmonotonic variation of the Griffiths dynamical exponent throughout the phase.

We now turn our attention to the phase boundaries between the three phases. The direct transition at weak intercolor coupling between the paramagnetic and ferromagnetic (Baxter) phases [transition (i) in Fig. 1] is in the infinite-randomness universality class of the random transverse-field Ising chain, as was already found in Refs. [19,21]. In contrast, the corresponding phase boundary in the clean quantum Ashkin-Teller chain shows an unusual line of fixed points with continuously varying exponents [18,27]. The quantum phase transitions separating the partially ordered phase from the paramagnetic and ferromagnetic phases [transitions (ii) and (iii)] are also of infinite-randomness type and in the universality class of the random transverse-field Ising chain, while they are in the $(1 + 1)$-dimensional Ising universality class in the clean model.

We have also studied the quantum multicritical point separating the two-phase and three-phase regions. It is in one of two different universality classes (both of infinite-randomness type), depending on whether the intercolor coupling strengths

ϵ are uniform or random. This differs from the infinite-order multicritical behavior seen in the clean case [18,27].

Generalizations of the Ashkin-Teller Hamiltonian (1) to $n > 2$ colors have recently reattracted considerable attention because they have been used to analyze the fate of first-order quantum phase transitions under the influence of disorder [21,28,29]. Interestingly, for $n > 4$ colors, the paramagnetic and ferromagnetic phases meet directly at the self-dual line $\langle \ln h \rangle = \langle \ln J \rangle$ for all coupling strengths $\epsilon \geqslant 0$. Thus, an analog to the partially ordered strong-coupling phase does not exist. For three and four colors, this question is not yet solved to the best of our knowledge.

The random quantum Ashkin-Teller chain (1) with N sites can be mapped onto a random XXZ quantum spin chain with $2N$ sites [30]. Under this mapping, the transverse fields h_i in the Ashkin-Teller model map onto the even bonds of the XXZ chain while the interactions J_i map onto the odd bonds. The coupling strengths $\epsilon_{h,i}$ and $\epsilon_{J,i}$ map onto the local anisotropies of the XXZ chain. Importantly, the mapping is nonlocal as it involves (semi-infinite) chains of operators. Thus, although the energy spectra of the Ashkin-Teller model and the XXZ chain are analogous, their order parameters are not directly related. This explains, for example, why the correlation length exponent ν_ϵ given in Eq. (13) takes the same value as the exponent that describes the effects of weak anisotropy about the Heisenberg fixed point of the XXZ chain [10]. In contrast, our order parameter exponent β_ϵ does not have a direct counterpart in the XXZ chain.

Our study has focused on one space dimension. Let us briefly comment on random quantum Ashkin-Teller models in higher dimensions. The crucial step in our understanding of the strong-coupling regime was the transformation defined in Eqs. (2)–(7) from the original spins to the product variable. This transformation is purely local and can be performed in the same way in any space dimension. We therefore believe that the basic features of the phase diagram in higher dimensions will be similar to the one-dimensional case. In particular, for small ϵ, we expect a direct transition between the ferromagnetic and paramagnetic phases while a partially ordered product phase is expected to intervene between them for large ϵ. Obtaining quantitative results in higher dimensions will be significantly more complicated than in one dimension. First, the Hamiltonian is not self-dual in $d > 1$; thus, the phase diagram is not symmetric under the exchange of transverse fields and interactions. Second, the SDRG can only be implemented numerically in $d > 1$ because the decimation steps change the topology of the lattice. This work remains as a task for the future.

ACKNOWLEDGMENTS

This work was supported by the NSF under Grants No. DMR-1205803 and No. PHYS-1066293, by the Simons Foundation, by FAPESP under Grant No. 2013/09850-7, and by CNPq under Grants No. 590093/2011-8 and No. 305261/2012-6. R.N. acknowledges the hospitality of the Physics Department of Missouri S&T where this work was initiated. J.H. and T.V. acknowledge the hospitality of the Aspen Center for Physics.

APPENDIX A: SDRG RECURSION RELATIONS

A single step of the SDRG consists in identifying the largest local energy scale in the Hamiltonian and perturbatively integrating out the corresponding high-energy excitations. This is done using the projection technique described, e.g., in Ref. [31]. The Hilbert space is divided into a low-energy subspace and a high-energy subspace. Any wave function ψ can be decomposed as $\psi = \psi_1 + \psi_2$ with ψ_1 in the low-energy subspace and ψ_2 in the high-energy subspace. This allows us to write the Schrödinger equation in matrix form,

$$\begin{pmatrix} H_{11} & H_{12} \\ H_{21} & H_{22} \end{pmatrix} \begin{pmatrix} \psi_1 \\ \psi_2 \end{pmatrix} = E \begin{pmatrix} \psi_1 \\ \psi_2 \end{pmatrix}, \tag{A1}$$

with $H_{ij} = P_i H P_j$. Here, P_1 and P_2 project on the low-energy and high-energy subspaces, respectively. Eliminating ψ_2 from these two coupled equations gives $H_{11}\psi_1 + H_{12}(E - H_{22})^{-1} H_{21}\psi_1 = E\psi_1$. Thus, the effective Hamiltonian in the low-energy Hilbert space is

$$H_{\text{eff}} = H_{11} + H_{12}(E - H_{22})^{-1} H_{21}. \tag{A2}$$

The second term can now be expanded in inverse powers of the large local energy scale.

The quantum Ashkin-Teller Hamiltonian has four competing local energy scales, viz., J_i, K_i, h_i, and g_i, rather than two. We therefore generalize the usual SDRG scheme by considering the largest and second-largest energies in a local cluster to define the SDRG step. In the strong-coupling regime, $\epsilon > 1$, the largest local energy is always either a four-spin interaction or a two-spin field. In total, there are four possible steps.

(a) The largest local energy is a two-spin field g_i. The second-largest energy in the three-site cluster of sites $i - 1$, i, $i + 1$ is a four-spin interaction, either K_{i-1} or K_i. Let us assume that it is K_i for definiteness. In this case, the low-energy Hilbert space is spanned by states for which $(\eta_i, \sigma_i, \sigma_{i+1}) = (\rightarrow, \uparrow, \uparrow)$ or $(\rightarrow, \downarrow, \downarrow)$. H_{11} and H_{22} contain all terms in the Hamiltonian that do not flip the spins $\eta_i, \sigma_i, \sigma_{i+1}$; their leading terms are $-K_i \sigma_i^z \sigma_{i+1}^z - g_i \eta_i^z$. All terms that flip at least one of the variables $\eta_i, \sigma_i, \sigma_{i+1}$ are contained in H_{12} and H_{21}. Specifically,

$$\begin{aligned} H_{12} = P_1 \big[& - J_{i-1} \eta_{i-1}^z \eta_i^z - J_i \eta_i^z \eta_{i+1}^z - h_i \sigma_i^x - h_{i+1} \sigma_{i+1}^x \\ & - h_i \sigma_i^x \eta_i^x - h_{i+1} \sigma_{i+1}^x \eta_{i+1}^x - J_{i-1} \sigma_{i-1}^z \sigma_i^z \eta_{i-1}^z \eta_i^z \\ & - J_i \sigma_i^z \sigma_{i+1}^z \eta_i^z \eta_{i+1}^z \big] P_2. \end{aligned} \tag{A3}$$

H_{21} takes the same form but with P_1 and P_2 exchanged. We now insert H_{12} and H_{21} into Eq. (A2) and approximate the denominator $E - H_{22}$ by $-2g_i$ or $-2K_i$ depending on which of the spins $(\eta_i, \sigma_i, \sigma_{i+1})$ is flipped. The resulting effective Hamiltonian has the same form (8) as the initial one, but with one fewer site. The arrangement of the renormalized energies $\tilde{J}_{\text{eff}}$ and $\tilde{h}_{\text{eff}}$ between the remaining sites is shown in Fig. 2 and their values are given in Eqs. (9).

(b) Exactly the same SDRG step is carried out if the largest local energy is the four-spin interaction K_i, and the second-largest energy in the two-site cluster of sites i and $i + 1$ is a two-spin field, either g_i or g_{i+1}.

Steps (a) and (b) are the dominant SDRG steps for $\epsilon \gg 1$. More precisely, most steps are of types (a) or (b) if ϵ is larger

than the width of the h and J distributions (on a logarithmic scale). In the opposite case, strong disorder and not too large ϵ, most SDRG steps are site and bond decimations of types (c) and (d).

(c) The largest energy in the system is the two-spin field g_i, and the second-largest energy in the local cluster of sites $i-1$, i, and $i+1$ is the field h_i. In this case, the low-energy Hilbert space is spanned by all states having $(\eta_i,\sigma_i)=(\rightarrow\rightarrow)$. H_{11} and H_{22} contain all terms in the Hamiltonian that do not flip η_i and σ_i, with the leading terms being $-g_i\eta_i^x-h_i\sigma_i^x-h_i\eta_i^x\sigma_i^x$. All terms that flip η_i and/or σ_i are part of H_{12} and H_{21}. Specifically,

$$\begin{aligned}H_{12}=P_1\big[&-K_{i-1}\sigma_{i-1}^z\sigma_i^z-K_i\sigma_i^z\sigma_{i+1}^z-J_{i-1}\eta_{i-1}^z\eta_i^z\\&-J_i\eta_i^z\eta_{i+1}^z-J_{i-1}\eta_{i-1}^z\eta_i^z\sigma_{i-1}^z\sigma_i^z\\&-J_i\eta_i^z\eta_{i+1}^z\sigma_i^z\sigma_{i+1}^z\big]P_2,\end{aligned}\tag{A4}$$

and H_{21} takes the same form but with P_1 and P_2 exchanged. After inserting this into Eq. (A2) and approximating the denominator $E-H_{22}$ by $-2g_i-2h_i$ or $-4h_i$ depending on which spins are flipped, site i is eliminated (i.e., both σ_i and η_i are decimated). The effective interaction energies between the neighboring sites $i-1$ and $i+1$ are given in Eqs. (10).

(d) The largest local energy is a four-spin interaction K_i, and the second-largest energy in the cluster consisting of sites i and $i+1$ is the interaction J_i. The low-energy Hilbert space is spanned by states having $(\eta_i,\eta_{i+1},\sigma_i,\sigma_{i+1})=(\uparrow\uparrow\uparrow\uparrow)$ or $(\uparrow\uparrow\downarrow\downarrow)$ or $(\downarrow\downarrow\uparrow\uparrow)$ or $(\downarrow\downarrow\downarrow\downarrow)$. After projection into the low-energy Hilbert space, the two sites i and $i+1$ can thus be represented by a single site with variables $\sigma_{\rm eff}$ and $\eta_{\rm eff}$. H_{11} and H_{22} contain all terms in the Hamiltonian that do not flip η_i, η_{i+1}, σ_i or σ_{i+1}. The leading terms are $-K_i\sigma_i^z\sigma_{i+1}^z-J_i\eta_i^z\eta_{i+1}^z-J_i\sigma_i^z\sigma_{i+1}^z\eta_i^z\eta_{i+1}^z$. In contrast, H_{12} and H_{21} consist of the terms that flip η_i, η_{i+1}, σ_i, and/or σ_{i+1}. This gives

$$\begin{aligned}H_{12}=P_1\big[&-h_i\sigma_i^x-h_{i+1}\sigma_{i+1}^x-g_i\eta_i^x-g_{i+1}\eta_{i+1}^x\\&-h_i\eta_i^x\sigma_i^x-h_{i+1}\eta_{i+1}^x\sigma_{i+1}^x\big]P_2.\end{aligned}\tag{A5}$$

Inserting this into the effective Hamiltonian (A2) as before yields the transverse field $h_{\rm eff}$ and two-spin field $g_{\rm eff}$ acting on the cluster variables $\sigma_{\rm eff}$ and $\eta_{\rm eff}$. Their values are given in Eqs. (11).

Note that the SDRG steps (c) and (d) are identical to the site and bond decimations employed in the weak-coupling ($\epsilon<1$) analysis of Refs. [19,21].

APPENDIX B: MULTICRITICAL POINT

The multicritical point separating the two-phase and three-phase regions is located at $\delta=0,\epsilon=1$. In this appendix, we sketch the derivation of the SDRG flow on the self-duality line $\delta=0$ for $\epsilon>1$ but close to the multicritical point.

Let us begin with a qualitative discussion. For $\epsilon\approx1$ and strong disorder, initially almost all SDRG steps are site decimations (c) or bond decimations (d); thus, the RG flow is identical to that of the random transverse-field Ising chain. Under these steps, ϵ increases rapidly. When the typical $\ln\epsilon$ reaches the width of the $\ln J$ and $\ln h$ distributions, the character of the SDRG flow changes. Now, most steps are "mixed" decimations of types (a) and (b). Under these steps, the magnetization rapidly drops to zero while the polarization (product order parameter) stops decreasing and reaches a nonzero asymptotic value. Thus, the RG scale at which $\ln\epsilon$ reaches the width of the $\ln J$ and $\ln h$ distributions determines the correlation length and the polarization.

For a quantitative analysis of this SDRG flow, we start from the recursion relations for the coupling strengths $\epsilon_{J,i}$ and $\epsilon_{h,i}$ defined by Eqs. (10) and (11). Written in terms of logarithms, they read

$$\ln\tilde\epsilon_h=\ln\epsilon_{h,i}+\ln\epsilon_{h,i+1}+\ln[(1+\epsilon_{J,i})/2],\tag{B1}$$

$$\ln\tilde\epsilon_J=\ln\epsilon_{J,i-1}+\ln\epsilon_{J,i}+\ln[(1+\epsilon_{h,i})/2].\tag{B2}$$

We follow the ϵ flow from $\ln\epsilon\ll1$ to $\ln\epsilon\sim P_0^{-1},R_0^{-1}$ where P_0 and R_0 are the inverse widths of the $\ln J$ and $\ln h$ distributions. Two regimes need to be distinguished, $\ln\epsilon<1$ and $\ln\epsilon>1$.

For $\ln\epsilon<1$, we expand in $\delta^{(\epsilon)}=\ln\epsilon\approx\epsilon-1$, and Eqs. (B1) and (B2) simplify to

$$\tilde\delta_h^{(\epsilon)}=\delta_{h,i}^{(\epsilon)}+\delta_{h,i+1}^{(\epsilon)}+\tfrac12\delta_{J,i}^{(\epsilon)},\tag{B3}$$

$$\tilde\delta_J^{(\epsilon)}=\delta_{J,i-1}^{(\epsilon)}+\delta_{J,i}^{(\epsilon)}+\tfrac12\delta_{h,i}^{(\epsilon)}.\tag{B4}$$

The recursions can be understood as special cases of the general recursion $\tilde x_i=x_{i-1}+x_{i+1}+Yx_i$ with $Y=1/2$ [32]. The flow of variables governed by such recursions close to the infinite-randomness fixed point (of the random transverse-field Ising chain) was studied in detail by Fisher [10]. He found that the typical x scales like $\Gamma^{\phi_Y}=[\ln(\Omega_I/\Omega)]^{\phi_Y}$ with decreasing SDRG energy scale Ω. The exponent ϕ_Y is given by $\phi_Y=[1+(5+4Y)^{1/2}]/2$. [In contrast to Eqs. (16), we need to use the "asymmetric" version of Fisher's results because all our $\delta^{(\epsilon)}>0$.] Thus, in the first regime ($\ln\epsilon<1$), the typical $\ln\epsilon$ scales as

$$\ln\epsilon_{\rm typ}\approx\Gamma^{\phi_{1/2}}\ln\epsilon_0,\qquad\phi_{1/2}=\tfrac12(1+\sqrt7).\tag{B5}$$

In the second regime, $\ln\epsilon>1$, we can approximate the recursions (B1) and (B2) for $\delta^{(\epsilon)}=\ln\epsilon$ by

$$\tilde\delta_h^{(\epsilon)}=\delta_{h,i}^{(\epsilon)}+\delta_{h,i+1}^{(\epsilon)}+\delta_{J,i}^{(\epsilon)},\tag{B6}$$

$$\tilde\delta_J^{(\epsilon)}=\delta_{J,i-1}^{(\epsilon)}+\delta_{J,i}^{(\epsilon)}+\delta_{h,i}^{(\epsilon)}.\tag{B7}$$

These recursions are of the same type as Eqs. (B3) and (B4), but with $Y=1$. Thus, in the second regime, $\ln\epsilon$ scales as

$$\ln\epsilon_{\rm typ}\sim\Gamma^{\phi_1},\qquad\phi_1=2.\tag{B8}$$

To test the predictions (B5) and (B8), we implemented the strong-disorder renormalization group numerically. Figure 6 shows $(\ln\epsilon_{\rm typ})^{1/2}$ as a function of Γ for systems located on the self-duality line $h_{\rm typ}=J_{\rm typ}$. We employed identical power-law distributions $P_I(J)=J^{-1+1/w}/w$ and $R_I(h)=h^{-1+1/w}/w$ for the interactions ($0<J<1$) and transverse fields ($0<h<1$), with w being a measure of the disorder. The coupling strength is uniform and close to the multicritical value $\epsilon_I=1$. The figure shows that the data in the range $\langle\ln(\epsilon)\rangle>1$ lie on straight lines; i.e., they follow Eqs. (B8) as predicted. For $\langle\ln(\epsilon)\rangle<1$ the data curve downward, suggesting a smaller

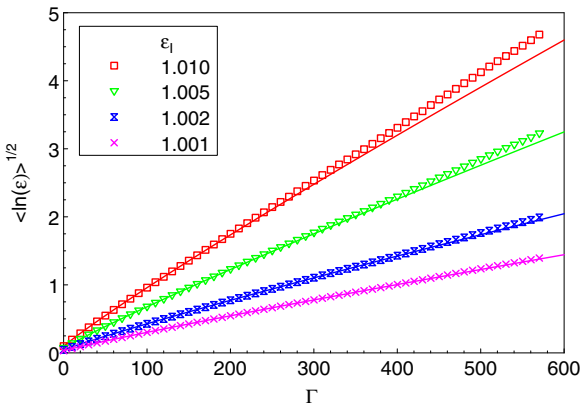

FIG. 6. (Color online) $\langle \ln(\epsilon) \rangle^{1/2}$ vs Γ for four different systems on the self-duality line $h_{\rm typ} = J_{\rm typ}$ close to the multicritical point ($w = 8$ and $\epsilon_I = 1.001$, 1.002, 1.005, and 1.01). Each curve stems from a single long chain of 2.5×10^7 sites. The solid lines are fits of the data in the range $\langle \ln \epsilon \rangle < 0.5$ to $\langle \ln \epsilon \rangle = C(\Gamma - \Gamma_0)^{\phi_{1/2}}$ with $\phi_{1/2} \approx 1.823$; see Eq. (B5).

exponent. In fact, the data in the range $0 < \langle \ln(\epsilon) \rangle < 0.5$ can be very well fitted with functions of the form $\langle \ln \epsilon \rangle = C(\Gamma - \Gamma_0)^{\phi_{1/2}}$, in agreement with Eqs. (B5).

Let us now combine the two regimes. We consider a (bare) system close to the multicritical point, $0 < \ln \epsilon_I \ll 1$, with strong initial disorder; i.e., the widths of the bare distributions of $\ln J$ and $\ln h$ are large, $P_I^{-1} = R_I^{-1} \gg 1$. Under repeated site and bond decimations [SDRG steps (c) and (d)], $P_0^{-1} = R_0^{-1} = P_I^{-1}\Gamma$ while the typical $\ln \epsilon$ scales as $\ln \epsilon \sim \Gamma^2 (\ln \epsilon_I)^{2/\phi_{1/2}}$ once $\ln \epsilon > 1$. Setting $\ln \epsilon = P_0^{-1}$ gives the crossover SDRG scale

$$\Gamma_x = \frac{1}{P_I (\ln \epsilon_I)^{2/\phi_{1/2}}}. \tag{B9}$$

The correlation length is given by the length scale corresponding to Γ_x,

$$\xi \sim \ell_x \sim \Gamma_x^2 \sim (\ln \epsilon_I)^{-4/\phi_{1/2}} \approx (\epsilon_I - 1)^{-4/\phi_{1/2}}. \tag{B10}$$

The correlation length exponent ν_ϵ thus takes the value $\nu_\epsilon = 4/\phi_{1/2}$ as given in Eqs. (13). The product order parameter (polarization) M_p can be found by noting that σ clusters are not decimated anymore once $\Gamma > \Gamma_x$. M_p is thus given by its value at Γ_x,

$$M_p = n(\Gamma_x)\, \mu(\Gamma_x) \sim \Gamma_x^{-2+\phi_0} \sim (\ln \epsilon_I)^{2(2-\phi_0)/\phi_{1/2}}, \tag{B11}$$

where $n(\Gamma)$ and $\mu(\Gamma)$ are the number and moment of clusters surviving at SDRG scale Γ. Using $\phi_0 = [1 + \sqrt{5}]/2$ yields the order parameter exponent β_ϵ given in Eqs. (13).

[1] D. S. Fisher, Phys. Rev. Lett. **69**, 534 (1992).
[2] D. S. Fisher, Phys. Rev. B **51**, 6411 (1995).
[3] M. Thill and D. A. Huse, Physica A **214**, 321 (1995).
[4] H. Rieger and A. P. Young, Phys. Rev. B **54**, 3328 (1996).
[5] T. Vojta, Phys. Rev. Lett. **90**, 107202 (2003).
[6] T. Vojta, J. Phys. A **39**, R143 (2006).
[7] T. Vojta, J. Low Temp. Phys. **161**, 299 (2010).
[8] S. K. Ma, C. Dasgupta, and C. K. Hu, Phys. Rev. Lett. **43**, 1434 (1979).
[9] F. Igloi and C. Monthus, Phys. Rep. **412**, 277 (2005).
[10] D. S. Fisher, Phys. Rev. B **50**, 3799 (1994).
[11] G. Theodorou and M. H. Cohen, Phys. Rev. Lett. **37**, 1014 (1976).
[12] L. C. Tippie and W. G. Clark, Phys. Rev. B **23**, 5846 (1981).
[13] T. G. Rappoport, L. Ghivelder, J. C. Fernandes, R. B. Guimarães, and M. A. Continentino, Phys. Rev. B **75**, 054422 (2007).
[14] P. Bak, P. Kleban, W. N. Unertl, J. Ochab, G. Akinci, N. C. Bartelt, and T. L. Einstein, Phys. Rev. Lett. **54**, 1539 (1985).
[15] V. Aji and C. M. Varma, Phys. Rev. Lett. **99**, 067003 (2007); Phys. Rev. B **79**, 184501 (2009).
[16] Z. Chang, P. Wang, and Y.-H. Zheng, Commun. Theor. Phys. **49**, 525 (2008).
[17] J. Ashkin and E. Teller, Phys. Rev. **64**, 178 (1943).
[18] M. Kohmoto, M. den Nijs, and L. P. Kadanoff, Phys. Rev. B **24**, 5229 (1981).
[19] E. Carlon, P. Lajkó, and F. Iglói, Phys. Rev. Lett. **87**, 277201 (2001).
[20] Even if we assume uniform, nonrandom values of ϵ_J and ϵ_h, they will acquire randomness under renormalization.
[21] P. Goswami, D. Schwab, and S. Chakravarty, Phys. Rev. Lett. **100**, 015703 (2008).
[22] The position of this phase boundary is fixed by the self-duality of the Hamiltonian.
[23] The extra factors of 2 in the denominator are irrelevant in the low-energy limit.
[24] We call this exponent κ rather than ψ (as was done in Ref. [10]) to avoid confusion with the tunneling exponent.
[25] Our exponent λ is equivalent to the exponent λ used in Ref. [10] to describe the scaling of the average anisotropy in an XXZ spin chain.
[26] F. Igloi and J. Solyom, J. Phys. A **17**, 1531 (1984).
[27] R. Baxter, *Exactly Solved Models in Statistical Mechanics* (Academic Press, New York, 1982).
[28] R. L. Greenblatt, M. Aizenman, and J. L. Lebowitz, Phys. Rev. Lett. **103**, 197201 (2009).
[29] F. Hrahsheh, J. A. Hoyos, and T. Vojta, Phys. Rev. B **86**, 214204 (2012).
[30] F. C. Alcaraz, M. N. Barber, and M. T. Batchelor, Ann. Phys. **182**, 280 (1988).
[31] A. Auerbach, *Interacting Electrons and Quantum Magnetism* (Springer, New York, 1998).
[32] x_i comprises both site and bond ϵ, arranged in an alternating fashion.